Compensation for Non-linear Iris Pattern Deformation based on the Tensile Properties of Iris

[1]Dae Sik Jeong, [1]Dalho Cho, [2]Jihye Jo, [2]Min-Kyeong Bae, [2]Min Woo Park, and [2]Eui Chul Lee*
[1]Laboratory of Counterfeit Banknote Detection, Kisan Electronics Co., LTD.
273-1 Seongsu 2-Ga, 3-Dong, Seongdong-Gu, Seoul, Republic of Korea
[2]Department of Computer Science, Sangmyung University
7 Hongji-Dong, Jongno-Gu, Seoul, Republic of Korea
*Corresponding author: eclee@smu.ac.kr

Abstract: - In general, iris recognition can be performed to identify users based on the unique iris patterns between their pupils and scleras. The main function of iris is to control the size of the pupil according to the amount of environmental light. Therefore, the iris patterns dilate and contract based on changing lighting conditions. To guarantee robust recognition accuracy in spite of these deformed iris patterns, previous research has used the linear rubber band model and uniform track allocation in iris regions. However, some iris patterns are actually deformed nonlinearly due to the complicated movements of certain iris muscles including the sphincter and the dilator. To overcome these problems, we propose a new method of extracting iris features by nonlinear and dynamic track allocation. This proposed method is based on the nonlinear tensile properties of iris patterns. This paper presents two contributions over previous works. First, we automatically detected the nonlinear positions of the iris patterns in the radial direction when the pupil dilated and contracted with changing illumination conditions. This was possible because we used a template matching process with five iris patches. From the process, we were able to allocate tracks in the iris region nonlinearly and dynamically. We then extracted robust iris features for recognition. Second, we found that the nonlinear tensile properties of the iris patterns differed individually. Based on that, we adopted a user-dependent method of dynamic track allocation, which greatly improved recognition accuracy. Experimental results showed that the accuracy of the proposed method was superior to that of conventional methods which use uniform track allocations based on the linear rubber band model.

Key-Words: Iris recognition, Tensile properties of iris patterns, Dynamic track allocation.

1 Introduction

In recent years, rapid developments in science and technology have made it possible to use biometrics in applications such as passenger control in airports, access control in restricted areas, and border control points, where it is often necessary to establish or confirm individual identities [1-3]. Iris recognition, which is based on the unique iris patterns of every individual, is considered to be one of the most reliable biometric systems [2-4]. The main function of iris patterns is to control the size of the pupil and thus control the amount of light entering the retina in widely varying illumination conditions. In general, the human pupil acts as an aperture in the optical system of the eye. The pupil size varies according to illumination changes. During this process, the pupil's diameter ranges from a minimum of about 1.5mm to a maximum of over 7mm [5]. Consequently, the iris texture patterns dilate and contract according to the changing environmental light. In previous research, in order to guarantee robust recognition accuracy against the deformations of iris patterns, Daugman used the linear rubber band model and uniform track allocation in iris regions [1-4]. However, the deformed iris patterns were actually nonlinear due to the complicated movements of certain iris muscles including the sphincter and the dilator, as shown in Fig. 7 and 8. Studies on iris physiology have also illustrated that the response of the texture with respect to different light intensities is non-linear due to the distribution of the iris muscles controlling the pupil size [14]. To overcome such problems, in previous research, Yuan and Shi used an iris meshwork model proposed by Wyatt [5][7]. Based on that model, the researchers found the relationship of iris collagen fibers with the different pupil sizes [7]. Li used a local calibration method in order to reduce iris distortion [9]. All of the above methods used Daugman's linear iris normalization method [1-4]. However, linear iris normalization cannot cover nonlinear deformations of iris patterns according to the dilation and contraction of a pupil. In other research, to overcome this problem, and

motivated by Wyatt's iris mesh model, Zhuoshi *et al*. adopted a nonlinear deformation correction algorithm that used a Gaussian function to approximate the additive deviation of nonlinear iris stretching [6]. However, these researchers did not automatically detect the nonlinearly moved position of the iris patterns in the radial direction when the pupil dilated and contracted. In addition, they used the same nonlinear deformation correction algorithm for all the users, and did not consider individual differences. In Clark *et al*.'s research, they analyzed non-linearity of iris muscle [23]. However, the research was performed based on only mathematical model. That is, experimental investigation was not performed. Actually, the standardized iris nonlinearity cannot be adopted into all persons.

To overcome these problems, we propose a new method of extracting iris features by nonlinear and dynamic track allocation based on the nonlinear tensile properties of iris patterns. In our research, we automatically detected the nonlinearly moved position of the iris patterns in the radial direction when the pupil dilated and contracted by using template matching with five iris patches. From that, we allocated tracks in the iris region nonlinearly and dynamically, and then extracted robust iris features for recognition.

In addition, we found that the nonlinear tensile properties of the iris patterns were different individually. Thus, we used the user-dependent method of dynamic track allocation, which could improve the recognition accuracy. Section 2 outlines the proposed method and experimental results are shown in section 3. In section 4, conclusions follow.

2 Proposed Method

2.1 Overview

Fig. 1 shows the overall procedure of the proposed method. After iris recognition started, for enrollment,

we used the proposed method to capture successive iris images by turning on and off the visible light illuminator (as shown in Fig. 2), in order to observe iris contractions and relaxations. Then, the proposed method was used to detect the inner and outer boundaries of the iris regions by eliminating the eyelash regions, the eyelid regions and the SR (specular reflections) (as shown in Fig. 1 (1)) [10-12]. We normalized the detected iris region into rectangular coordinates [1-4] (as shown in Fig. 1 (1)). Then, we detected the moved position of the iris patterns in the radial direction when the pupil dilated and contracted by using template matching with five iris patches (as shown in Fig. 1 (2)). Based on these detected positions, eight tracks were allocated in the iris region of the rectangular coordinates, dynamically and nonlinearly. From each track, we applied a Gabor filter and extracted

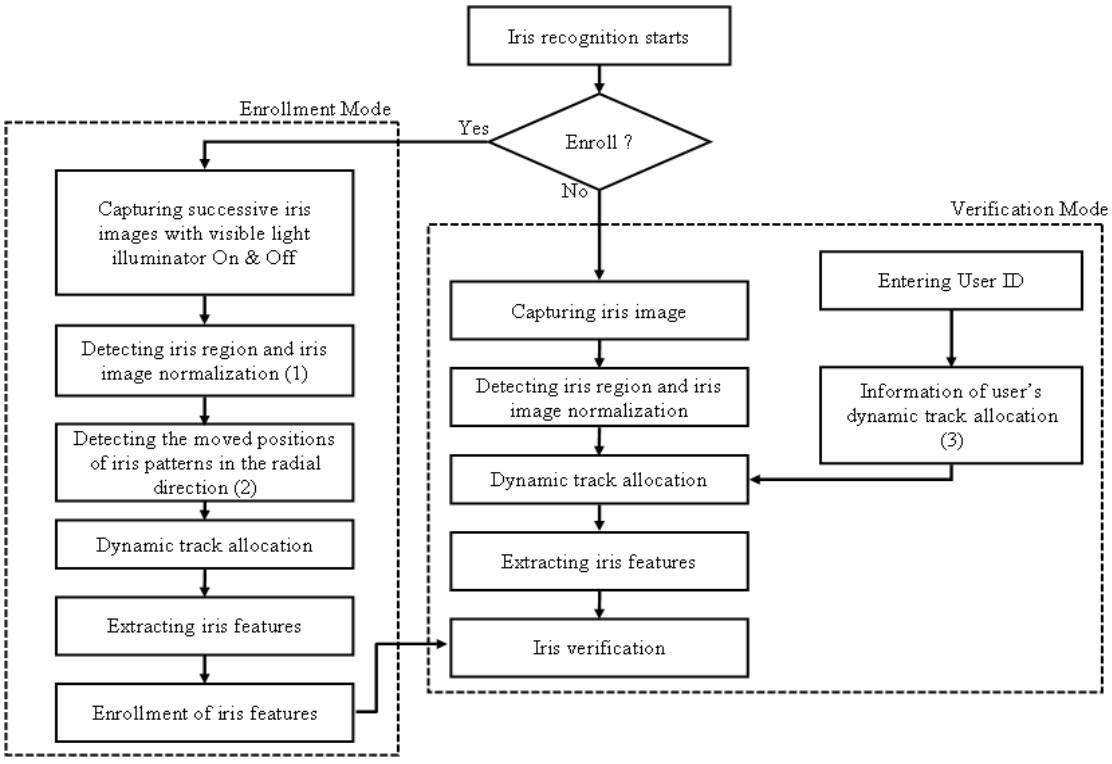

Fig. 1 Overall procedure of the proposed method

the iris binary codes. The extracted iris codes were then used for enrollment. For verification, we used the proposed method to capture the iris images. The same procedures of detecting the iris regions and normalizing the iris images were performed as in the enrollment mode. Then, with the user ID information, the user's dynamic track allocation information of Fig. 10 (c) was retrieved (as shown in Fig. 1 (3)). Based on this information, eight tracks were allocated in the iris region of the rectangular coordinates, both dynamically and nonlinearly. For each track, we applied a Gabor filter and extracted the iris binary codes as same manner to those in case of enrollment. The extracted iris codes were used for matching with the enrolled ones for authentication.

2.2 Enrollment Procedure

2.2.1 Capturing successive iris images with the visible light illuminator on and off

As shown in Fig. 1, in order to extract the by nonlinear deformation properties of iris patterns, we had to capture successive iris images turning on and off the visible light illuminator. At first, when we started the iris recognition procedure, we turned on the visible light illuminator for a predetermined time (experimental results showed that it was determined as two seconds) and the iris camera captured a total of 30 image frames at a speed of 15 frames per second. In general, visible light can be dazzling to users and can cause great inconvenience.

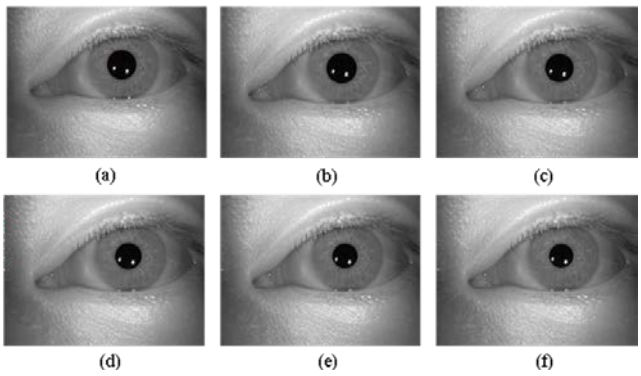

Fig. 2 Successive iris images captured by the proposed system with a visible light illuminator (6 image samples which were selected from 30 captured ones)

To solve this problem, we compared the user inconveniences in case of using different visible light illuminators such as red, orange, yellow, or violet. Subjective tests with 50 users showed that green light produced fewer dazzling effects than other colors and so, we used it for our system. Fig. 3 shows our proposed iris camera system. Because the iris camera included an IR (Infra-red) light passing filter in front of the camera lens, it cut off the visible light and passed through the IR light with a wavelength over 730 nm. Based on that, the visible light was not included in the captured image and we found that the pupil contracted with the visible light as shown in Fig. 2.

The visible light illuminator turned on during two seconds and it turned off after that. During the time when the visible light illuminator was turned on, the iris camera (shown in Fig. 3) captured 30 successive image frames with a near-infrared (NIR) light illuminator (with wavelengths of 750 nm and 850 nm). We used left and right NIR illuminators (as shown in Fig. 3), because single illuminator can make large specular reflections (SR) on the surface of glasses in case of user wearing glasses. And the large SR can hide iris regions, which degrades the user verification performance. For iris enrollment, in order to obtain a good quality iris image, the user was required to take off his or her glasses and a single (left or right) NIR illuminator was used to capture successive images with the visible light illuminator. However, for iris verification, in order to improve convenience, the user was permitted to keep his or her glasses on. Then, when the left illuminator made large SR on the surface of the glasses, our system turned it off and turned on the right illuminator and captured the iris image for verification. For iris verification, the visible light illuminator did not turn on and it was only used for iris enrollment (as shown in Fig. 1).

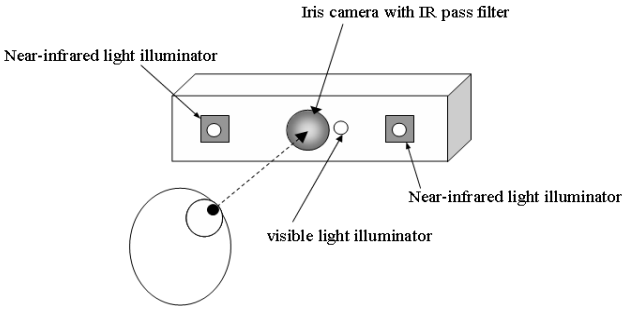

Fig. 3 Proposed iris camera system (A visible light illuminator and a single NIR illuminator were used for iris enrollment. Left and right NIR illuminators were used for iris verification)

2.2.2 Extracting the iris, pupil, eyelid and eyelash regions and image normalization in the polar coordinates

After capturing successive iris images, our system detected the iris regions (as explained in section 2.1 and shown in Fig. 1). Accurate extraction of the iris regions is a very significant part of iris recognition [13]. To extract accurate iris regions, we performed the following three steps (as shown in Fig. 4).

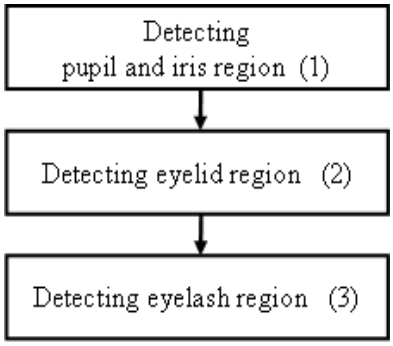

Fig. 4 Preprocessing steps when extracting iris regions

As shown in Fig. 4 (1), we rapidly located the pupil and iris regions of the images based on two circular edge detection methods [10], which was based on the conventional integro-differential circular edge detection [1-4]. Then, the upper and lower eyelids were detected by multiple local derivative masks and the parabolic curve fitting method (as shown in Fig. 4 (2)) [11].

From the detected iris, pupil and eyelid regions, we located the eyelash region based on eyelash detection masks and the characteristics of eyelash connectivity (as shown in Fig. 4 (3)) [12]. Detailed explanations of detecting iris, pupil, eyelid and eyelashes can be found in [10-12]. Fig. 5 shows the resulting images when detecting the iris, pupil, eyelid and eyelash regions.

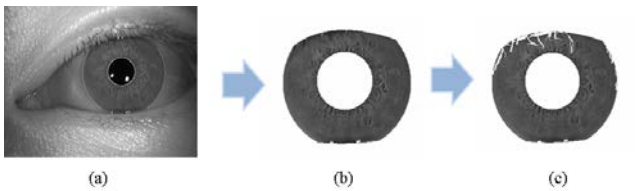

Fig. 5 The resulting images when detecting the iris, pupil, eyelid and eyelash regions Detecting the iris and pupil regions (b) Detecting the eyelid regions (c) Detecting the eyelash regions

The detected circular iris region was normalized in the polar coordinates in order to reduce the variance caused by rotation, translation and scaling of the iris image (as shown in Fig. 6) [12][17].

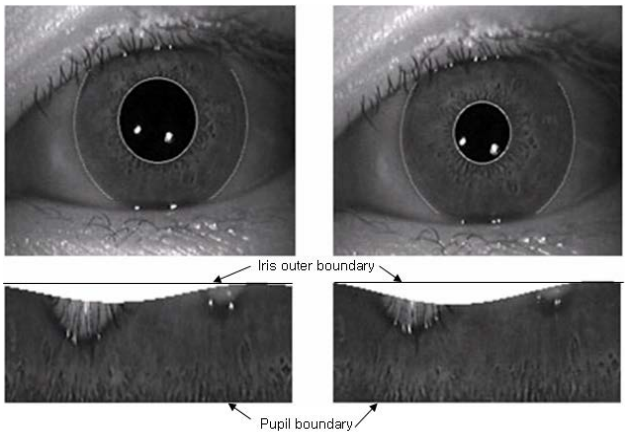

Fig. 6 Iris regions in the polar coordinates

2.2.3 Extracting the nonlinear tensile property of the iris patterns and dynamic track allocation

In iris textures, there are two dominant muscles in the angular and radial directions. The former muscle is known as the sphincter (circular fiber) and the latter muscle is known as the dilator (radial fiber), as shown in Fig. 7 [5]. In strong illumination conditions, the sphincter muscles close to the pupil region contract but the dilator muscles relax. In weak illumination conditions, the sphincter muscles relax but the dilator muscles contract.

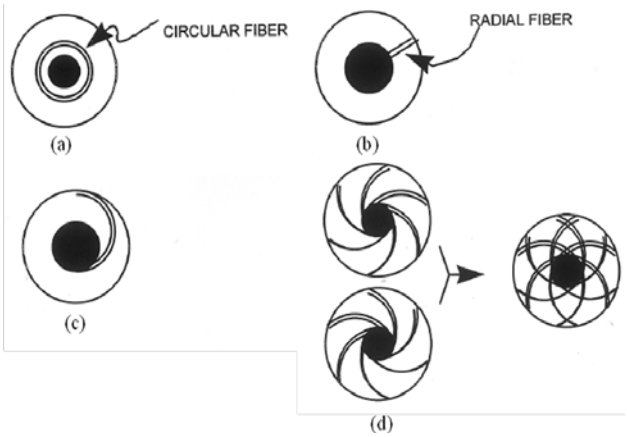

Fig. 7 The muscle structure of the iris [5] (a) A circular structural component in the iris that hinders pupil dilation. (b) A radial component that hinders pupil constriction. (c) A semicircular structural component in the iris. (d) A meshwork of left-and right-handed arcs, as described by Rohen [16].

Based on that, as illumination conditions change, iris textures such as the circular muscle and the radial muscle show different variations of contraction and relaxation. This causes the nonlinear deformation of the iris patterns according to the dilation and contraction of the pupil (as shown in Fig. 8).

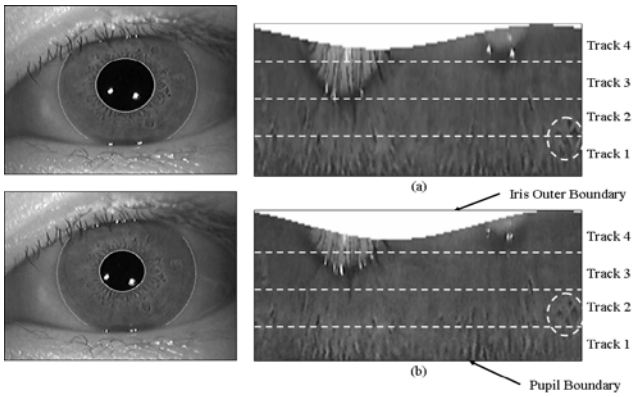

Fig. 8 The nonlinear deformation of iris patterns (a) Pupil dilation (b) Pupil contraction

In Fig. 8, we defined five tracks of uniform width from the pupil boundary based on Daugman's linear rubber band model [1-4]. The positions of the iris patterns changed in each track with pupil dilation and contraction (see the dotted circles in Fig. 8 (a) and (b)). Such nonlinear positional changes degrade the recognition accuracy when we used the linear rubber band model.

To overcome this problem, we used the dynamic track allocation method with a non-uniform track width. For that, we extracted five patches of iris textures in the iris image (in which the pupil was dilated with the visible light off as shown in Fig. 8 (a) and Fig. 9).

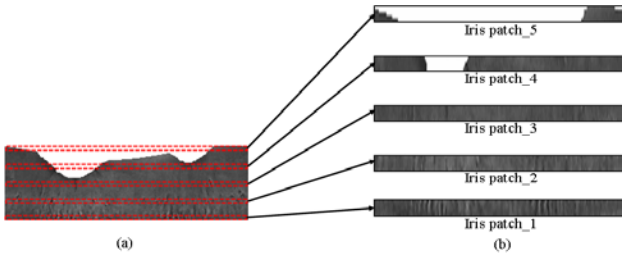

Fig. 9 The extracted five iris patches (a) Iris image with pupil dilation (b) Extracted iris patches

In detail, we extracted iris patches 2, 3, and 4 in the regions between tracks 1 and 2, tracks 2 and 3, and tracks 3 and 4, respectively. Iris patches 1 and 5 were extracted in the regions close to the pupil and the outer boundaries. Iris patches 1 and 2 roughly represent the movements of the circular muscles in the area close to the pupil boundary. Iris patches 3, 4 and 5 roughly represent the movements of the radial muscles.

The size of each iris patch was 5 (height) × 512 (width) pixels. By using the five iris patches, we performed template matching in the radial direction with the successive images, which were captured with the visible light illuminator on and off (as shown in Fig. 2). In order to increase the performance of template matching, brightness normalization was done based on the mean gray level of the iris region before template matching. Based on the best-matched positions of the five iris

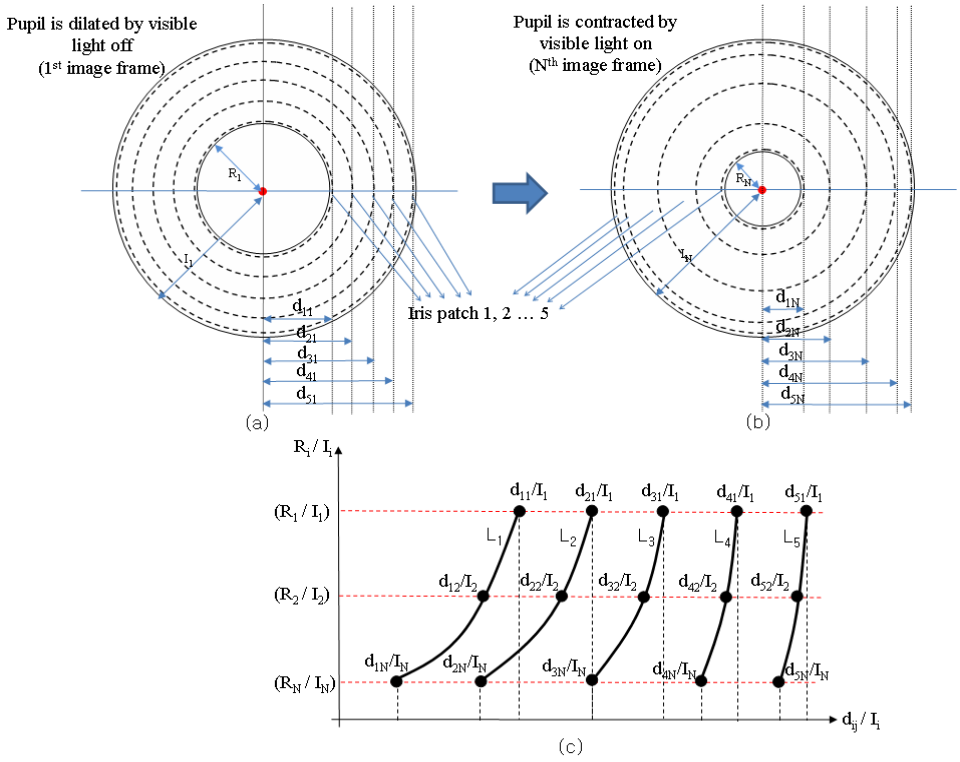

Fig. 10 The dynamic track allocation information (a) Iris image with pupil dilation (b) Iris image with pupil contraction (c) The dynamic track allocation information

patches, we obtained the dynamic track allocation information (as shown in Fig. 10).

As shown in Fig. 10, the five iris patches were extracted in the image in which the pupil was dilated by visible light off. From that, we obtained the five distances shown as d_{11}, d_{21}, … d_{51}. With the five iris patches, we performed template matching and obtained the positions of the five iris patches shown as d_{1N}, d_{2N}, … d_{5N} (where N means the N^{th} image frame and we regarded N as 30) with the successive captured images (of Fig. 2). For template matching, we also considered eye rotation and the templates were matched in both the horizontal and vertical directions within a predetermined range in the iris images of the polar coordinates (as shown in Fig. 11).

One optimal shift value in the horizontal direction was determined from the weight sum of five shift values from five templates. If the template included occluded regions such as eyelid, eyelash and specular reflections, then it had a lower weight compared to that without such occluded area.

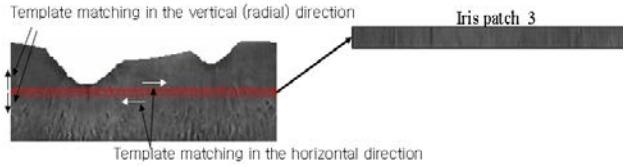

Fig. 11 Template matching in the horizontal and vertical directions (with iris patch 3)

From those templates, we obtained the nonlinear graph for dynamic track allocation as shown in Fig. 10 (c). Although we used 30 frames to obtain this graph, the procedure took less than 10ms when using a Pentium-IV 2 GHz because only five iris patches were used for template matching. In the dynamic track allocation graph of Fig. 10 (c), we normalized the R_i and d_{ij} by I_i (the radius of the iris) because the lengths of R_i and d_{ij} were also changed by the zooming factor of the human iris according to the Z distance between the user's eye and the iris camera as well as the pupil dilation and contraction procedures. Based on the five nonlinear curves shown as L_1, L_2 … L_5 in Fig. 10 (c), we determined four tracks in the iris region. The region between L_1 and L_2 is the 1^{st} track and that between L_2 and L_3 is the 2^{nd} track and so on.

In order to compare the performance of the proposed method to Daugman's method [1-4], we expanded eight tracks from the four tracks and extracted iris features in each track. For the expansion, we modeled the distribution of the inter-distance between L_N and L_{N+1} as a Gaussian one based on [6]. Then, we segmented each track of Fig. 10 (c) into two tracks and obtained eight tracks consequently. For example, the 1^{st} track between L_1 and L_2 is divided into 2 tracks and so on. 2.2.4 Extracting the iris codes with the Gabor wavelet filter for enrolment.

We segmented each of the eight tracks into 256 sectors based on [1-4] and applied a 1D Gabor wavelet filter to each sector in order to extract the iris binary codes. The Gabor filter ($G(x)$) was defined as Eq. (1):

$$G(x) = A \cdot e^{-\pi\left[\frac{(x-x_0)^2}{\sigma^2}\right]}(cos\{2\pi[u_0(x-x_0)]\} \quad (1)$$

where A represents the amplitude of Gabor filter. σ and u_0 are the kernel size and the frequency of the Gabor filter, respectively.

To ensure that the generated iris code was not changed by the image brightness of the iris texture, we set the DC component of the Gabor filter as 0 [17]. The kernel size and frequency were selected in order to minimize the EER (Equal to Error Rate) when testing with the CASIA-IrisV3-Lamp DB [20]. If the convolved value obtained by the Gabor wavelet filter was positive, then we assigned it a value of 1. If it was negative, then 0 was assigned. From that, we obtained the iris code of 2048 bits from eight tracks and 256 sectors. If the iris code was extracted from an occluded region, we regarded it as invalid and it was not used for code matching. Then, our system saved the extracted iris code of 2048 bits and the dynamic track allocation information (of Fig. 10 (c)) for each person.

Experimental results showed that the dynamic track allocation information was different for each person. In the research discussed in [21-22], it was mentioned that generally both the circular and radial components undergo large changes in stretching as the pupil size changes, since each person has a different stretching rate for their iris muscles. So, we used different dynamic track allocation information for each person, whereas Wei *et al*. [6] used the same information in their research.

2.3 Verification Procedure

When the iris image was captured, our system located the iris region by the same manner discussed in section 2.2.2. With the detected value of R/I (as shown in Fig. 10 (c)) and the retrieved dynamic track allocation information based on the user ID (as shown in Fig. 1 (3)), the proposed system determined the eight non-uniform tracks in the iris regions. From that, the proposed system extracted the iris codes and tried to match them with the enrolled ones. Iris code matching was performed based on the HD (Hamming Distance) [1-4] using the XOR operation, as shown in Eq. (2).

$$HD = \frac{\|(codeA \otimes codeB \cap maskA \cap maskB \|}{\|maskA \cap maskB \|} \qquad (2)$$

where $\otimes$ is the simple Boolean Exclusive-OR operator (XOR), and $\cap$ is the AND operator, respectively. The HD value was calculated by the two-phase iris code bit denoted code A and code B in Eq. (2). Mask A and mask B calculated mask bits that noticed whether the extracted iris code was valid or non-valid. If the calculated distance was greater than the threshold, the user was rejected. If it was smaller than the threshold, the user was accepted as a genuine user. The threshold was determined based on authentic and imposter distributions and the Bayesian rule [17]. Experimental results showed the threshold to be 0.34.

3 Experimental Results

In the first test, we measured iris recognition accuracy when using the proposed method with the CASIA-IrisV3-Lamp database [20]. The images were collected by an OKI's IrisPass-h in an indoor environment with a visible lamp on/off. The numbers of subjects and classes were 411 and 819, respectively. Each class included 19 ~ 20 iris images which included the dilation and contraction of pupil according to a visible lamp on/off. The total number of images was 16,213. The image size was 640×480 pixels. Due to the visible lamp, the images showed the nonlinear deformation caused by the dilation and contraction of the pupil (as shown in Fig. 12). From the images of each class, three images were used for training (obtaining the dynamic track allocation information of Fig. 10). And, the others were used for testing. In details, we selected three images of each class (the size of pupil is smallest, medium and largest, respectively) and obtained the dynamic track allocation information of Fig. 10. And the others were used for testing.

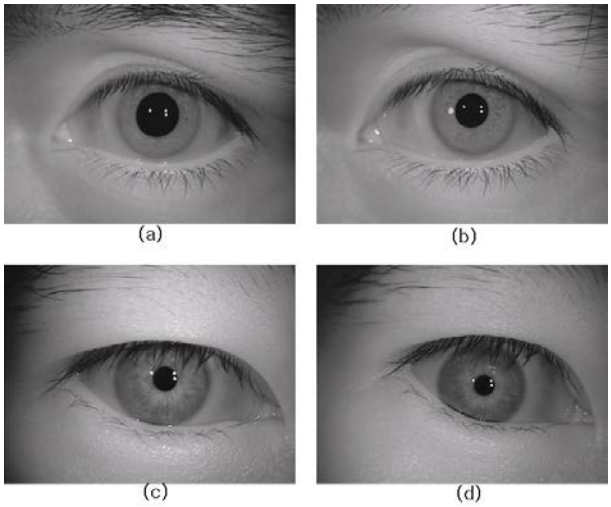

Fig. 12 The dilation and contraction of the pupil in the CASIA-IrisV3-Lamp database (a) and (c) the dilation of the pupil, (b) and (d) the contraction of the pupil

From that, we compared the iris recognition accuracy of the proposed method to of the accuracies of Daugman's linear rubber band model [4] and Wei's nonlinear track model [6]. The differences between the proposed method and Wei's method were that we used a different nonlinear track model for each person and we also used automatic detection of the nonlinear deformation positions of each track based on template matching (see section 2.2.3 and 2.2.4). Table 1 shows the EER (Equal Error Rate) of each method. The EER can be defined as the smallest error rate which is obtained when the FAR (False Acceptance Ratio) and the FRR (False Rejection Ratio) are the same.

Table 1. Comparative iris recognition accuracies (EER (%)) of Daugman's [4], Wei's [6] and the proposed method (Using CASIA-IrisV3-Lamp database)

Daugman's method [4]	Wei's method [6]	Proposed method
0.932	0.714	0.621

From Table 1, it is clear that the proposed method showed better accuracy compared to the other methods. Even though we used the same CASIA-IrisV3-Lamp database, the performance of the measured EER values of Wei's method in our experiment were a little better than those in [6]. That is because we used different methods for iris, eyelid and eyelash detection [10-12]. According to the ROC (Receiver Operating Characteristic) curve of each method, we could know that the proposed

method showed better accuracy than other methods.
In the second test, we measured the comparative recognition accuracy rates of images from the iris database that were captured by our lab-made iris camera with the additional visible lamp on/off [8]. The numbers of subjects and classes were 50 and 100, respectively. Each class included ten images and the consequent number of iris images was 1,000. The image size was 640×480 pixels. Fig. 13 shows some samples of captured images.

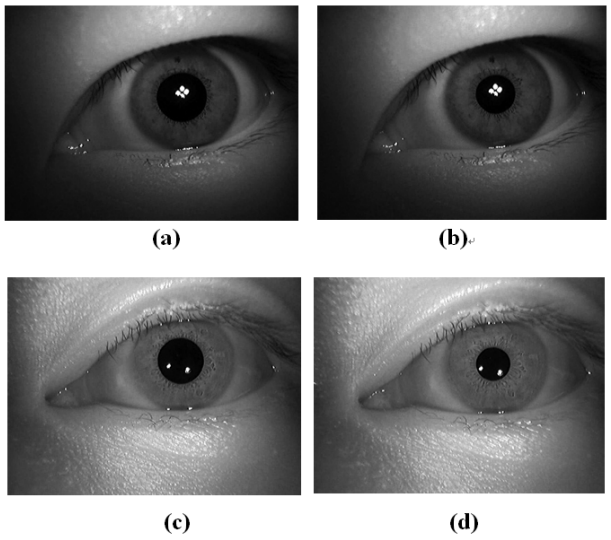

Fig. 13 The dilation and contraction of the pupil in the captured images (a) (c) the dilation of the pupil (b) (d) the contraction of the pupil

Table 2. Comparative iris recognition accuracies (EER (%)) of Daugman's [4], Wei's [6] and the proposed method (with iris images captured by our lab-made iris camera with the additional visible lamp on/off [8])

Daugman's method [4]	Wei's method [6]	Proposed method
0.521	0.412	0.365

From Table 2, it is clear that our method showed better accuracy compared to the other methods. In addition, according to the ROC curve of each method, we could know that our method showed better accuracy compared to the other methods.
The accuracy in case of using iris images captured by our lab-made iris camera was superior to that using CASIA-IrisV3-Lamp database. That was because the iris diameter (200 ~ 220 pixels) of the images captured by our lab-made iris camera was greater than that (200 or less than 200 pixels) of CASIA-IrisV3-Lamp database as shown in Fig. 12 and 13.

Processing time was as small as 250ms for iris enrollment and 92ms for iris verification with a Pentium-IV 2 GHz CPU. An additional two seconds were required for iris enrollment in order to capture thirty successive images in which dilation and contraction of the pupil occurred (see section 2.2.1).

4 Conclusions

In this paper, we proposed a new method of extracting iris features by nonlinear and dynamic track allocation based on the nonlinear tensile properties of iris patterns. Experimental results with two kinds of databases showed that the accuracy of our method was superior to the accuracy of Daugman's and Wei's methods.
In future work, we plan to do more tests with iris images in which the pupil is dilated and contracted by sunlight in outdoor conditions. In addition, we plan to apply active contour tracks instead of circular tracks in the detected iris region.

Acknowledgements

This work was supported by a NAP (National Agenda Project) of the Korea Research Council of Fundamental Science &Technology.

References:

[1] D. Impedovo, G. Pirlo, and L. Scianatico, "Regional Approach for Iris Recognition," *WSEAS Transactions on Information Science and Applications*, Vol. 11, 2014, pp. 61-71.
[2] J. G. Daugman, "High Confidence Visual Recognition of Personals by a Test of Statistical Independence," *IEEE Trans. Pattern Analysis Machine Intelligence*, Vol. 15, No. 11, 1993, pp. 1148-1160.
[3] J. G. Daugman, "Demodulation by Complex-valued Wavelets for Stochastic Pattern Recognition," *International Journal of Wavelets, Multi-resolution and Information Processing*, Vol. 1, No. 1, 2003, pp. 1-17.
[4] J. G. Daugman, "How Iris Recognition Works," *IEEE Trans. on Circuits and Systems for Video Technology*, Vol. 14, No. 1, 2004, pp. 21-30.
[5] H. J. Wyatt, "A 'minimum-wear-and-tear' Meshwork for the Iris," *Vision Research*, Vol. 40, 2000, pp. 2167-2176.
[6] Z. Wei, T. Tan, and Z. Sun, "Nonlinear Iris Deformation Correction Based on Gaussian Model," *Lecture Notes in Computer Science on ICB 2007*, Vol. 4642, 2007, pp. 780-789.
[7] X. Yuan, and P. Shi, "A Non-linear Normalization Model for Iris Recognition," *Lecture Notes in Computer Science on IWBRS*

2005, Vol. 3781, 2005, pp. 135-141.

[8] B. J. Kang, and K. R. Park, "Restoration of Motion-blurred Iris Image on Mobile Iris Recognition Devices", *Optical Engineering*, Vol. 47, No. 11, 2008, pp. 117202-1 - 117202-8.

[9] X. Li, "Modeling Intra-class Variation for Non-ideal Iris Recognition," *Lecture Notes in Computer Science*, Vol. 3842, 2006, pp. 419-427.

[10] D. Cho, K. R. Park, D. W. Rhee, Y. Kim, and J. Yang, "Pupil and Iris Localization for Iris Recognition in Mobile Phones," *Proceeding of SNPD*, Las Vegas, USA, 2006.

[11] Y. K. Jang, B. J. Kang, and K. R. Park, "A Study on Eyelid Localization Considering Image Focus for Iris Recognition," *Pattern Recognition Letters*, Vol. 29, No. 11, 2008, pp. 1698-1704.

[12] B. J. Kang, and K. R. Park, "A Robust Eyelash Detection Based on Iris Focus Assessment," *Pattern Recognition Letters*, Vol. 28, Issue 13, 2007, pp. 1630-1639.

[13] G. O. William, "Iris Recognition," *IEEE Aerospace and Electronics Systems Magazine*, Vol. 12, No. 4, 1997, pp. 23-29.

[14] P. C. Bressloff, C. V. Wood, and P. A. Howarth, "Nonlinear Shunting Model of the Pupil Light Reflex," *Proc. Royal Soc. B*, Vol. 263, 1996, pp. 953-960.

[15] http://www.newmediarepublic.com/dvideo/compression/adv09.html (accessed on 17th June, 2015).

[16] H. Rohen, Der Bau der Regenbogenhaut beim Menschen und einigen Säugern, *Gegenbaur Morphology Journal*, Vol. 91, 1951, pp. 140–181.

[17] H. A. Park, and K. R. Park, "Iris Recognition Based on Score Level Fusion by Using SVM," *Pattern Recognition Letters*, Vol. 28, Issue 15, 2007, pp. 2019-2028.

[18] K. Hanna, R. Mandelbaum, L. Wixson, D. Mishra, and V. Paragana, "A System for Non-intrusive Human Iris Acquisition and Identification," *Proceeding of IAPR Workshop on Machine Vision Applications*, Tokyo, Japan, 1996, pp. 200-203.

[19] N. Macmillan, and C. Creelman, *Detection theory: A Users Guide*, New York: Cambridge University Press, 1991.

[20] http://www.cbsr.ia.ac.cn/english/Databases.asp (accessed on 2015. 06. 17).

[21] A. Muron, and J. Pospisil, "The Human Iris Structure and its Usages," *Acta Univ. Palacki. Olomuc, Fac. Rer. Nat. Physica*, Vol. 39, 2000, pp. 87-95.

[22] E. R Berman, "Biochemistry of the Eye," *Springer*, 1991.

[23] M. J. Burge, and K. W. Bowyer, "Handbook of Iris Recognition," *Springer*, 2013.